REVIEW

Graphene/molybdenum disulfide nanocomposites: characterization and optoelectronic application

Nagham M. Obaid, Amer Al-Nafiey,* and Ghaleb Al-Dahash
University of Babylon, College of Sciences for Woman, Babylon, Iraq

Abstract. The ability to modify and shape the surface of polymer and composite materials is crucial for a number of biological and electronics applications. Molybdenum disulfide (MoS_2) and graphene are two-dimensional materials that have distinctive electrical and optical properties that are useful in many optoelectronic applications. The latest applications of graphene/MoS_2, as well as heterostructure manufacturing, properties, and applications, are discussed. Heterostructured materials, as opposed to single-component materials, are designed to provide additional functionality or flexibility. Our study focuses on their unique traits and capabilities, as well as applications, notably in the field of photodetector technology. [DOI: 10.1117/1.JNP.17.010901]

Keywords: graphene; molybdenum disulfide; properties; optoelectronics.

Paper 22083V received Aug. 30, 2022; accepted for publication Dec. 8, 2022; published online Jan. 4, 2023.

1 Introduction

The chemical type and structure of a material's components are recognized to have a significant impact on its properties.[1] Bulk materials that contain a large number of atoms, in particular, can be identified by the energy bands that are responsible for most of the physical and chemical properties of solid materials due to the overlapping of atomic and molecular orbitals. As for nanomaterials with dimensions ranging from 10 to 100 nm, the number of atoms is so small that the electronic energy bands change dramatically, affecting all physical properties of materials.[2–4]

Silicon and germanium structures are nanostructured semiconductors that emit visible light luminescence despite having modest and indirect band gaps in their bulk state.[4] The PL signals appear to be dependent on the size of the nanostructures, implying that the quantum confinement process is involved.[4,5]

On the other hand, metals with nanostructures are known to have a variety of unique characteristics. Metallic nanoparticles (NPs) show marked differences in color when their size and shape differ, as well as changes in transmitted and reflected spectra.[6] These color effects are linked to individual metal NPs' efficient resonant absorption of light and the stimulation of localized surface plasmons, which are associated with metal electron collective oscillations.[6]

This review will look at the many ways of producing nanomaterials based on MOS_2 and graphene for device manufacturing and optoelectronics applications, such as mechanical exfoliation, liquid exfoliation, and chemical vapor deposition (CVD).

2 Nanocomposite

Metallic NPs implanted in a dielectric multitude are significantly influenced by their physical and chemical characteristics, such as their distribution within the matrix and attributes such size, shape, or size dispersion. As a result, controlling these characteristics during manufacturing has long been a difficulty, and one of the biggest obstacles to the development of useful applications based on these materials has been the lack of production techniques with the required level of control.[7] This review will focus on the following nanomaterials.

*Address all correspondence to Amer Al-Nafiey, amer76z@yahoo.com

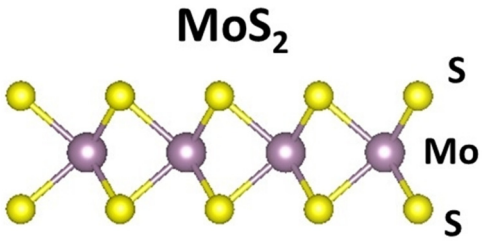

Fig. 1 MOS_2 structure.[8]

2.1 *Molybdenum Disulfide*

Among 2D materials, the TMD family has received the most attention.[8] TMDs are hexagonal in nature and absorb visible- to infrared-ranged light.[9] They are promising semiconducting materials with extremely thin bodies that enhance carrier confinement and electrostatic gate control as a result of programmable bandgaps and the absence of surface dangling bonds.[8] This study focuses on molybdenum disulfide (MoS_2), a well-known and thoroughly investigated TMD material with Mo atoms sandwiched between two layers of S atoms that has environmental stability and natural availability (Fig. 1).[8,10]

Moreover, it appears in nature as an n-type material,[11] with visible to near-infrared light absorption,[9] a large work function of 5.1 eV,[12] and mechanical stability and transparency for flexible devices.[8]

The most attractive feature of MOS_2 is the variable energy gap from 1.2 to 1.8 eV as the material moves from the bulk indirect bandgap to the direct bandgap monolayer due to the quantum confinement effect.

Furthermore, MoS_2 has optical properties that are thickness dependent.[13–15] The number of layers in MoS_2 influences its electron affinity. The monolayer MoS_2 had an electron affinity of 4.0 eV,[16] three layers of MoS_2 had an affinity of 4.0 eV,[17] and multilayers (28 nm) had an affinity of 4.1 eV.[18] Thus the MoS_2, with a monolayer thickness of 0.65 nm, has more than 80% of its transparency, making it ideal for wearable applications.[19] The MoS_2's physical properties are given in Table 1.

As mentioned, the contact Schottky barrier height, contact resistivity, and carrier mobility are all impacted by thickness.[8] Depending on the application, the MoS_2 layer's thickness needs to be carefully adjusted for maximum performance. MoS_2 nanofiber bundles were made by the hydrothermal technique in 2007 by Nagaraju et al.,[24] using ammonium molybdate in an acidic medium and maintained at 180°C for several hours. The sample's PXRD pattern may be easily identified as hexagonal 2H-MoS_2. According to the MoS_2 FTIR spectra, the band at 480 cm^{-1} is called (Mo-S). MoS_2 nanofibers are found in bundles that are 20 to 25 m long and 120 to 300 nm in diameter.

According to Li et al.,[25] advanced materials for photoelectrochemical water splitting are essential for the field of renewable energy. This study demonstrated selective solvothermal synthesis of MoS_2 NPs on sheets of reduced graphene oxide (rGO) floating in solution. The

Table 1 Physical properties of the MoS_2.

Property	Value
Charge carrier mobility	Up to 200 $cm^2/V \cdot s$[20]
Molar mass	160.07 g/mol[21]
Band gap	1.8 eV (direct)[22]
Specific density	5.06 g/cm^3[21]
Melting point	2648 K[23]

resulting MoS_2/rGO hybrid material, in contrast to the enormous aggregated MoS_2 particles grown freely in solution without GO, had nanoscopic few-layer MoS_2 structures with a lot of exposed edges piled on graphene. The MoS_2/rGO hybrid demonstrated greater electrocatalytic activity in the hydrogen evolution process when compared with conventional MoS_2 catalysts [hydrogen evolution reaction (HER)].

The study by Helmly et al.[26] investigated the production and characterization of molybdenum (IV) chalcogenide NPs. The process involves the interaction of molybdenum hexacarbonyl with sulfur or selenium. The NPs absorb light in the UV area of the spectrum, whereas bulk molybdenum (IV) chalcogenides absorb light in the near-IR. When stimulated in the UV range, the particles also emit a blue fluorescence.

Also Li et al.[27] used temporally structured femtosecond laser ablation of bulk MoS_2 targets in water to create monolayer MoS_2 QDs. The findings of the investigation reveal that very pure, homogeneous, and monolayer MoS_2 QDs may be produced effectively.

A combination of multilayer photoexfoliation of monolayer MoS_2 and water photoionization enhanced light absorption is the underlying process. Because of the many active edge sites, high specific surface area, and superior electrical conductivity, the as-prepared MoS_2QDs have remarkable electrocatalytic activity for hydrogen evolution processes. The second important material for postsilicon electronics that are used in optoelectronics applications is MoS_2.[27]

MoS_2 NPs were generated using the laser ablation technique (Nd:YAG = 1064 nm) in the polymer ethylene glycol solution as a function of laser fluence, according to Moniri and Hantehzadeh.[28] The resulting NPs are hexagonal crystals with diameters ranging from 4 to 160 nm, according to the findings. Furthermore, according to the laser fluence, the majority of them had a maximum wavelength that ranged from 212.5 to 216.5 nm. As the laser flux increases, the size of these particles will increase from 10 to 18 nm.

2.2 *Graphene*

Graphene, as shown in Fig. 2, is the basic structure of all forms of graphite that is now used in most modern fields in the last decade. As a result of its unusual physical and chemical features, it has piqued the interest of researchers all over the world, proving its theoretical significance.[30] The physical characteristics of graphene are provided in Table 2.

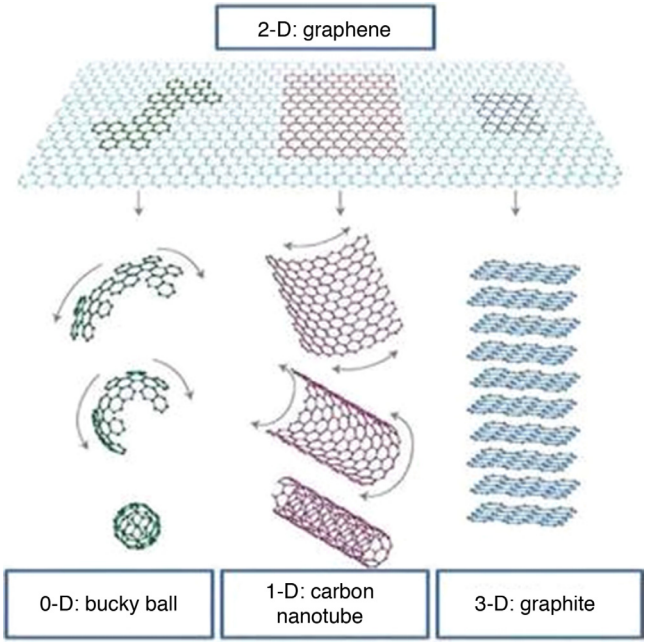

Fig. 2 Structure of graphene.[29]

Table 2 Physical properties of graphene.[31]

Property	Value
Charge carrier mobility	~200,000 $cm^2/V \cdot s$
Thermal conductivity	(3 to 5) 10^3 $W/m \cdot K$
Transparency	~97.4%
Specific surface area	~2630 m^2/g
Young's modulus	~1 TPa
Tensile strength	~1100 GPa
Band gap	0
Specific density	2.26 g/cm^3
Resistivity	2.26 $\mu\Omega \cdot cm$
Thermal stability	450°C to 650°C
Melting point	3800 K
Current density	>10^8 A/cm^2

3 Synthesis Methods for 2D Materials

To obtain high performance, two-dimensional materials must be synthesized with large dimensions, adjustable thicknesses, and few crystal defects.[32] Mechanical exfoliation, liquid exfoliation, CVD, laser ablation, and pulsed-laser deposition (PLD) have all been used to make 2D materials. A quick description of how these methods work is given below.

3.1 *Mechanical Exfoliation Technique*

The mechanical exfoliation technique is a method that involves extending layered materials by outside forces (such as chemical or physical forces) to lessen interlayer noncovalent interactions connections, allowing them to gradually separate into a single structure of very few layers.[33] The first synthesis method for making graphene was the method of mechanical exfoliation, known as the adhesive tape method; it has since been successfully used for multilayer 2D materials. The few-layer MoS_2 nanosheets were generated by Li et al.[34] utilizing an exfoliation technique, as shown in Fig. 3(a). A second sticky side of the tape was applied to the scotch tape with crystal after the first one was pushed onto the crystal surface for about 5 s. The scotch tape is then carefully removed at the tiniest possible angles. The two tapes are then torn, and crystals of the same size are glued to each. When this procedure is repeated, the bulk MoS_2 flakes become thinner and thinner until they are reduced to one or a few layers. The MoS_2 layers on tape were next successfully adhered to a spotless Al_2O_3 ceramic substrate. Before removing the scotch tape, the adhesion state was maintained for 6 h. After that, acetone was poured over the substrate to eliminate the scotch tape's adhesive residue. It is a simple, inexpensive, and straightforward technology for creating high-quality 2D materials, but it has limitations due to the size of the created material being <100 m and the inability to change the layer thickness. As a result, it is unsuitable for materials research and device demonstration at the industrial level in pioneering work.

3.2 *Liquid Exfoliation Technique*

The liquid exfoliation method is an inexpensive method. Hernandez[36] used sonication to exfoliate graphite in an organic solution containing N-methyl pyrrolidone. The graphene dispersion was obtained at a concentration of 0.01 mg/ml, and a monolayer graphene yield was 1 wt.%.

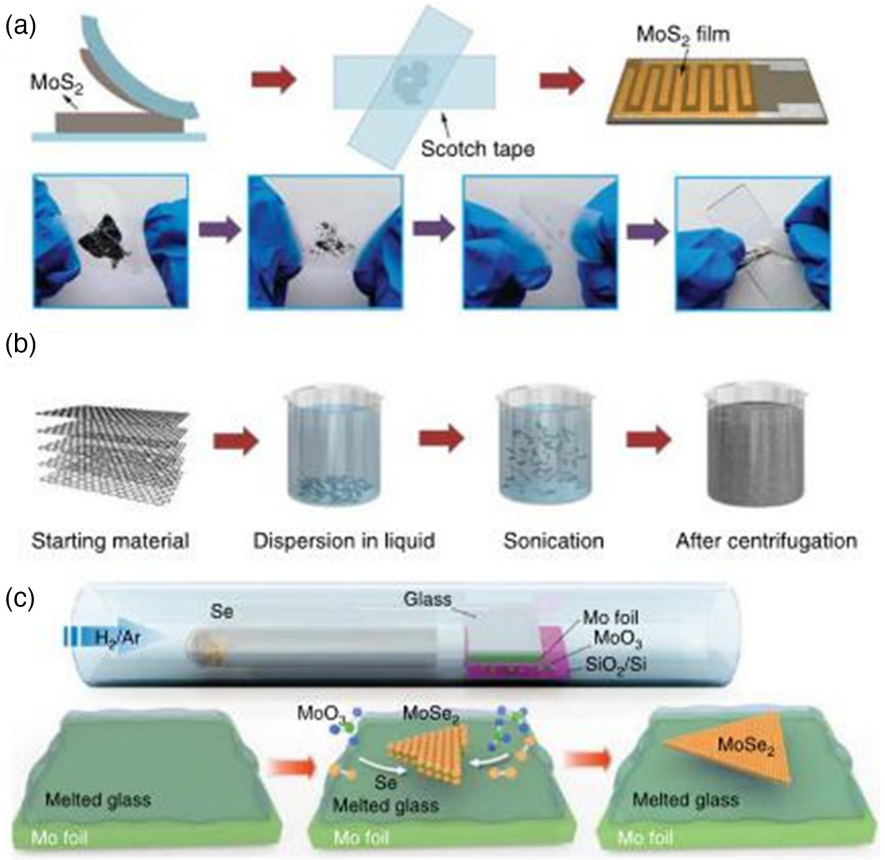

Fig. 3 (a) Diagram of the mechanically exfoliated MoS_2 nanosheets,[30] (b) a schematic of the liquid exfoliation process's mechanism, and (c) diagram of the CVD method used to create $MoSe_2$ crystals on molten glass.[35]

Various liquid exfoliation procedures, such as high shear mixing,[35] microoxidization,[37] and jet cavitation,[38] have been documented. As illustrated in Fig. 3(b), sonication-assisted liquid exfoliation is widely used in synthesis. Nanosheets are created simply by dissolving the beginning bulk material in a solvent to disperse the two-dimensional components in the solution, and ultrasound or centrifugation is used.

3.3 *Chemical Vapor Depositions Technique*

Using active chemical reactions of precursors in a designed environment, CVD is used to create 2D materials. Numerous operational factors, such as substrates, the position of substrates, carrier gas, pressure, temperature, and flow rate, require in-depth knowledge and engineering to produce crystals of high quality.[32,39] Chen et al.[40] used CVD to rapidly create high-quality millimeter-sized monolayer $MoSe_2$ crystals on molten glass. As shown in Fig. 3(c), glass substrates were placed inside a quartz tube that was installed inside an oven. To contain the molten glass, a piece of SiO_2/Si was used with Mo sheets, which are placed the above the MoO_3 source.

3.4 *Pulse Laser Ablation Technique*

The laser ablation technique is one of the most effective physical methods for producing NPs. The principle of this technique is summarized by absorbing the laser beam falling on the surface of a solid target, which leads to the expulsion of its components and the formation of nanostructures. When the solid target is removed in a vacuum or gas, nanoclusters are deposited on a substrate placed at a distance from the solid target (usually a few centimeters). When the ablation is carried out in a liquid environment (e.g., water, ethanol, and acetone), the NPs are released into

the liquid medium and form a colloidal nanosolution. The properties of the resulting nanostructures can be controlled by different laser parameters (wavelength, pulse duration, laser energy, and number of pulses) as well as by the properties of the medium liquid.[41]

3.5 *Pulsed-Laser Deposition Technique*

When material is ablated from a solid target in a gaseous environment, it can be recovered as a powder or as a deposit on a substrate. Although some uses, such as fuel cell applications of carbon nanotubes and nanohorns,[42] necessitate the manufacture of nanostructured powders, the majority of applications necessitate the deposition of thin nanostructured films.[43] The traditional PLD technology was found to be well suited for these jobs as it does not need any synthetic cluster size selection. The ablation of material is commonly conducted in PLD nanofabrication investigations using a nanosecond excimer laser (KrF and ArF) operating at UV wavelengths (248 and 193 nm, respectively) or the second harmonic of a Nd:YAG laser, as illustrated in Fig. 3 (532 nm). Because these wavelengths are lightly absorbed by plasma, they have little impact on the ablation process. At an incidence angle of roughly 45 deg, the radiation is focused on the surface of a revolving target (e.g., Si). The radiation intensity is typically between 108 and 109 W/cm. The plume of the laser-induced plasma extends perpendicular to the target surface. The substrates are placed at a distance (usually a few centimeters) from the target on a rotatable substrate holder. To increase the adherence of the deposited substance, the substrate is either held at room temperature or heated. The deposition is done in the presence of residual inert (He and Ar) or reactive (O and N) gases, at a low pressure (about 0.01 to 20 Torr), prior to filling with gases (Fig. 4).

4 Optoelectronics

A branch of photonics known as optoelectronics (or optronics) studies uses electronic devices and systems that source, detect, and control light. Light is often used to refer to both visible and invisible radiations in this context and includes gamma rays, x-rays, ultraviolet (UV), and infrared rays. Optoelectronic devices are electrical-to-optical or optical-to-electrical transducers or instruments that use such devices.[44] The quantum mechanical effects of light on electronic materials, particularly semiconductors, in the presence of electric fields are the basis of optoelectronics.[45]

5 Photodetector Parameters

In general, the performance of a photodetector is determined by some of the key parameters listed below.[46–49]

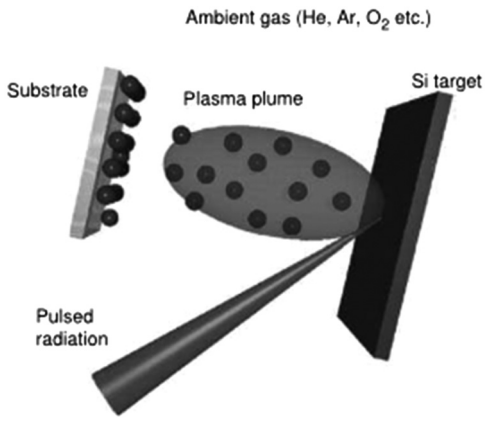

Fig. 4 Schematic of the PLD experiment for Si-based nanostructured film deposition.

5.1 *Sensitivity (R)*

The ratio of photocurrent (I_{ph}) via the detector to input light power $P_{optical}$, where $I_{ph} = I_{illuminated} - I_{dark}$ is

$$\frac{I_{illuminated} - I_{dark}}{P_{optical}} \text{ (A/W)}.$$

5.2 *External Quantum Effectiveness*

The proportion of charge carriers captured by the photodetector to incident light is the external quantum effectiveness (EQE), which is influenced by the material coefficient and the thickness of the absorbing material:

$$\frac{hc}{e\lambda}R.$$

5.3 *On/Off Ratio*

The proportion of photocurrent to dark current is the on/off ratio. The device should have a high on/off ratio because this indicates an improved photocurrent and reduced dark current, both of which increase device noise. The on/off ratio is calculated as

$$\frac{I_{ph}}{I_{dark}}.$$

5.4 *Detection Specificity (D∗)*

The photodetector's responsivity and dark current determine how feeble a light the gadget can detect. Dark current should be reduced to the greatest extent possible because it makes it difficult to distinguish very weak optical signals and adds to the device's noise; it is expressed as follows, where Δf is the electrical bandwidth, n is the noise current, and A is the effective area of the detector:

$$\frac{(A\Delta f)^{1/2}.R}{i_n} \text{ (Jones)}.$$

5.5 *Response Time*

The rise and fall times of the optical signal response range from 10% to 90% and 90% to 10% of the maximum photocurrent, respectively.

5.6 *Power Equivalent to Noise*

The NEP is the incident power required to achieve a signal-to-noise ratio of 1 at 1 Hz bandwidth, as determined by the noise spectral density.

6 Photodetectors Based on Two Dimensional Materials

6.1 *Graphene-Based Photodetectors*

The photoconductor and photovoltaic effects lie at the heart of graphene PDs. The external bias voltage is not required for graphene PDs because the high conductivity of graphene may create a huge dark current. A metal–graphene Schottky junction can be used to add built-in electric fields. Xia et al.[50] was the first to announce graphene PD with a bandwidth of 40 GHz and a

photoresponsivity of 0.5 mA/W. Most PDs have a low response[51] or high dark current due to the graphene channel bias[52] or fabrication method.[53]

In addition, Huang et al.[54] discovered that the graphene/HfO/Si photodetector has a significantly greater interfacial gating effect than the graphene/SiO/Si photodetector. The graphene/HfO/Si photodetector has a photo responsivity of 45.8 A/W.

By modifying the rGO film with hydrophilic polymers, Shih et al.[55] demonstrated a feasible method for designing surface homogeneity and improving photodetector performance. The on/off ratio of the PVA/rGO photodetector is 3.5 times higher than that of the rGO photodetector, and the detective improves by 53% even when the photodetector is operated at a low bias of 0.3 V.

6.2 *MoS_2-Based Photodetectors*

Graphene PDs when compared with 2D MoS_2-based PDs rely primarily on photovoltaic effects, resulting in higher responsivity and smaller dark currents. MoS_2 is one of the most thoroughly investigated TMDs because of its high carrier mobility of up to 200 cm^2/Vs, high absorption efficiency, and electrical operation (on/off) ratio of more than 10^8. As a result of quantum confinement, the bulk MoS_2 band gap can be converted from indirect to direct 1.2 to 1.8 eV by reducing it to a single layer.

Yin et al.[56] demonstrated a single-layer phototransistor prepared by the mechanical exfoliation method with a responsivity to light of 7.5 mA/W at a wavelength of 750 nm and a response time of about 50 ms. Following that, researchers observed that charge trapping in MoS_2, surface modification, preparation techniques, layer number, and the electrode contact all play a key role in MoS_2 PD performance.[57–60] Meanwhile, Selamneni et al.[61] established flexible broadband for all MoS_2 PD based on MoS_2 QDs and MoS_2 heterojunctions recently, with a responsivity (R) value of 12.8 mA/W and specific detectivity ($D*$) value of 7.2×10^9 Jones. Furthermore, Han et al.[62] created a MoS_2 PD with a responsivity (R) of 1.4×10^5 A/W and specific detectivity ($D*$) of 9×10^{15} Jones, both of which were many magnitudes greater than Si and Ge PDs.

Also Kumar et al.[63] constructed a highly effective UV photodetector based on MoS_2 layers using the PLD technology, with a $D*$ of 1.8×10^{14} Jones.

Recently, the photoelectric performance of the MoS_2/PSS photodetector was increased under three layers of 365, 460, and 660 nm.[64] The photocurrent rose thrice under the 365-nm laser, the noise equivalent power decreased to 1.77×10^{-14} $W/Hz^{1/2}$, and the specific detectivity ($D*$) increased by 1.2×10^{10} Jones.

Also Li et al.[65] described a waveguide-integrated MoS_2 photodetector functioning for hot electron-assisted photodetection to enable the telecom band. The low bias voltage of 0.3 V resulted in a photo responsiveness of 15.7 $mA\,W^{-1}$ at a wavelength of 1550 nm, which was also fairly uniform throughout the entire telecom band. Table 3 displays a comparison of MoS_2 production methods.[66]

6.3 *Photodetectors Based on Polymer–Graphene/MoS_2*

MoS_2 is considered to be a possible 2D material for optoelectronic applications due to its exceptional electrical and optical properties. The response range of MoS_2-based photodetectors can be increased using a semimetal material with a zero bandgap, such as graphene. Table 4 illustrates the various strategies for building a polymer/MoS_2/graphene-based photodetector.

6.4 *Solar Cell Based on MoS_2/Graphene*

Many photovoltaic applications use transition metal dichalcogenides (TMDCs), particularly MoS_2 with a 2H crystal structure.[74] The bandgap of TMDCs ranges from 1.0 to 2.0 eV, which corresponds to the Sun's spectrum and with solar cell based on semiconductors, such as Si (1.1 eV), GaAs (1.4 eV), and CdTe (1.5 eV).[75] It has been reported that 2D TMDCs with a thickness of 1 nm absorb 5% to 10% of incoming light per unit volume and have the absorption efficiency of the Sun that is greater than commonly used light absorbers such as Si and GaAs.

Table 3 Comparison of MoS_2 synthesis techniques.

Methods	Structures and layer numbers	Advantages	Disadvantages
Mechanical sloughing	A single layer of nanosheets	Appropriate for making individual devices	Low output Questionable layer numbers
Exfoliation using a laser	Nanosheets	Location and energy that can be controllable	Unknown scale
Sonic exfoliation	Quantum dots	High quality flexible layer	Unknown scale
		Large scale	Large size distribution
Shear exfoliation	Nanosheets (40 to 220 nm) Length (2 to 12) layers	Easy process Fast procedure	A wide range of sizes and thicknesses
Liquid intercalation	Nanosheets (1 to 8) layers	Higher monolayer energy	Required: flammable chemical (Li compound)
Hydrothermal	Nanoflowers	Low temperature High yield	Uncertain structure
CVD	Single or monolayer nanosheets lateral size up to several micrometers	Controllable layer numbers and size Large scale	High temperature

Table 4 Different methods for fabricating polymer/MoS_2/graphene-based photodetector.

Design	Year	Device fabrication approach	Application type	Responsivity (W/A)	Specific detectivity (Jones)	Reference
MOS_2/graphene heterostructure	2015	Facile hydrothermal	Photodetector	—	—	67
MOS_2/graphene	2015	G:ME MOS_2:ME	Photodetector	2.06×103	1.5×1015	17
Graphene/MOS_2/PE	2016	CVD	Photodetector	45.5	—	19
MOS_2/graphene	2018	CVD	Photodetector	33.3	—	68
Poly (3-hexylthiophene)/ graphene	2019	Spin-coating	Photodetector	0.25	1.8×108	69
MOS_2-PANI	2019	Internal polymerization of MOS_2	Photodetector	25	—	70
Graphene/MOS_2/ graphene	2019	G:CVD MOS_2:CVD	Photodetector	2	10^{13}	51
Graphene/MOS_2/ graphene	2020	G:CVD Dry transfer	Photodetector	2.2×10^5	3.5×10^{13}	71
Polymer–graphene	2020	Spin-coating	Gas detector	—	—	72
PVA/G/Ag	2021	PLAL	Photodetector	9.36	54.04	73
PMMA/G/Ag	2021	PLAL	Photodetector	15.6	90.06	73

The quantity of light absorbed by the TMDC single layer is equivalent to the amount absorbed by the 50-nm-thick Si layer, resulting in greater photocurrent values.[76]

In dye-sensitive solar cells, the antpolar plays an important role in the reduction process that occurs by transferring electrons through an external circuit. The electrocatalytic action of the counter electrode substantially influences the photo electrochemical process in dye-sensitized solar cells (DSSCs).[77] In DSSCs, MoS_2 is employed as a counter electrode instead of the conventionally used high-priced Pt electrodes.[78–80]

Lei et al.[81] employed MoS_2 as a counter electrode in three different structural: MoS_2 NPs, multilayered MoS_2, and few-layered MoS_2. The photon conversion efficiency of various MoS_2 morphologies is (5.41%) for MoS_2 NPs, (2.92%) for ML-MoS_2, and (1.74%) for FL-MoS_2.

Also Lin et al.[82] obtained a power conversion efficiency (PCE) of 6.07% as a counter electrode, and MoS_2 was implanted with graphene flakes. MoS_2 allows for a quick reduction of triiodide ions, and graphene flakes, which are extremely conductive, allow for a quick charge transfer. In 2012, the same team employed a MoS_2/rGO nanocomposite as the opposite electrode and achieved a PCE of 6.04%.[83]

Furthermore, MoS_2 was identified as an HTL rather than PEDOT:PSS (poly(4,8-bis[(2-ethylhexyl)oxy)[1,2-b:4,5-b]dithiophene-2,6-diyl-3-fluoro-2-[(2-ethoxyhexyl)-carbonyl][3,4-b] dithiophene-2,6-diyl-3-fluoro-2-[(2-ethoxyhexyl)-carbonyl]thiophenediyl) PTB7:PC71BM solar cells and (3-alkylthiophenes).[84] Organic solar cells based on P3HT:PC71BM ([6,6]-phenyl C71 butyric acid methyl ester) demonstrated a PCE of 8.11% and 4.02%, respectively. The PCE varies from 6.97% to 8.11% in PTB7:PC71BM-based solar cells when the layers of MoS_2 are changed, demonstrating the reliance of the PCE on the number of layers of MoS_2. The solar cell based on monolayer MoS_2 achieved the VOC = 0.69 V, the fill factor FF = 64%, the JSC = 15.78 mA/cm^2, and the PCE = 6.97%.

Li et al.[85] demonstrated that MoS_2 may be employed as an anode buffer layer in organic solar cells to avoid current leakage between ITO and PC61BM; the result was a PCE = 3.9%. Solar cells made of ITO without a buffer layer have a PCE = 2.14%. A nanocomposite of PEDOT:PSS/MoS_2 may be employed as a hole extraction layer in solar cells based on P_3HT:PCBM ([6,6]-phenyl-C61-butyric acid methyl ester) with a PCE = 3.74%.[86]

Yang et al.[87] employed MoS_2 as a hole layer in an organic solar cell. The organic solar cell PTB_7:$PC_{71}BM$ was employed as an active layer; PFN poly[(9,9-bis(3′-(N-N-dimethylamino)-propyl)-2,7-fluorene)-alt-2,7-(9,9dioctylfluorene)-alt-2,7-(9,9dioctylfluorene)-alt-2,7-9, in comparison with PEDOT:PSS, MoS_2 nanosheets and oxygen-containing MoS_2 nanosheets demonstrated superior optical transparency in range the wavelength 400 to 900 nm, with a PCE of 4.99%. This is due to the possibility of using graphene as layers for extracting electrons and holes in organic solar cells.

MoS_2 was used as both an electron extraction layer and a hole withdrawal layer.[88] P-type doped MoS_2 was used for the hole withdrawal layer, and n-type doped MoS_2 was used for the electron extraction layer. The photon conversion efficiency increased from 2.8% to 3.4% in organic solar cells using p-type doped MoS_2 as a hole extraction layer.

MoS_2 was used as an interfacial layer, and silver nanowires were used in conjunction with MoS_2 to create a transparent electrode.[89] At 550 nm, Ag NWs-MoS_2 exhibited 93.1% transparency as a transparent electrode and had a reduced sheet resistance 9.8/sq. When compared with the Ag NW electrode alone, MoS_2 in the Ag NWs-MoS_2 composite electrode enhanced environmental dependability and offered the best oxidation and moisture resistance. A PBDTTT-C-T:A PC70BM-based organic solar cell with a cathode made of Ag NWs-MoS_2 nanosheets/n-MoS_2 nanosheets and an anode made of p-MoS_2 nanosheets/Ag for hole extraction produced a PCE of 8.72%. As seen in Fig. 5(a), the general cell structure is glass/Ag-MoS_2/n-MoS_2/PBDTTT-C-T:$PC_{70}BM$/p-MoS_2/Ag.

Qin et al.[90] and Yang et al.[91] employed MoS_2 in conjunction with the MoO_3 layer and MoS_2 layer with Au NPs as hole extraction layers in solar cells. Also Chuang, et al.[92] used MoS_2 nanosheets with Au NP as an electron extraction layer, yielding a PCE = 4.91%. Jian et al.[93] investigated the role of the MoS_2 layer in graphene/silicon organic solar cells. MoS_2 was used as the interlayer in this case and provided a 4.4% PCE.

The same group[93] investigated the influence of annealing temperature on the PCE of the MoS_2 prototype. Tsuboi et al.[94] employed MoS_2 as an electron blocking and passivation layer

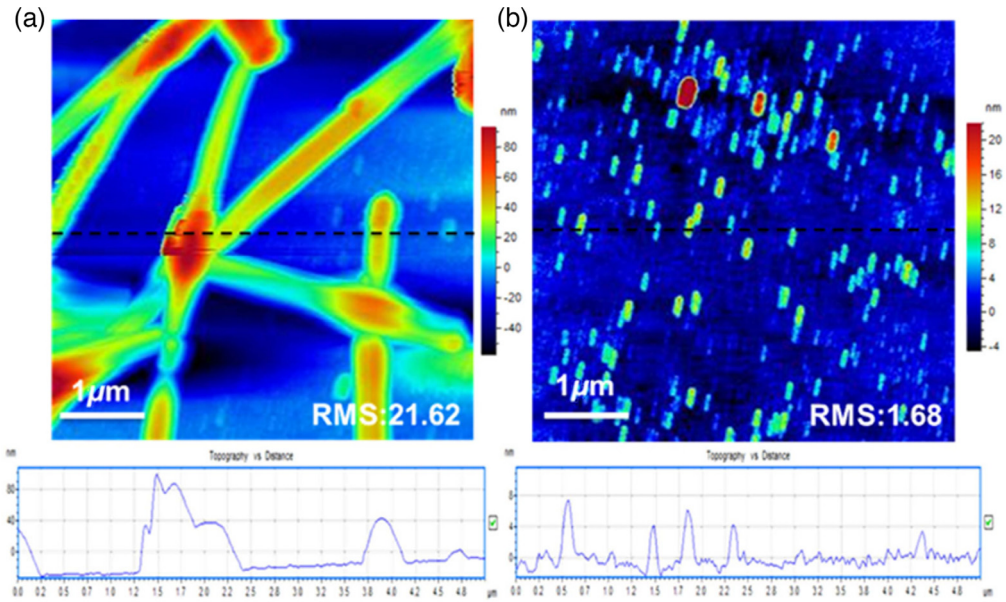

Fig. 5 Tapping-mode AFM images of electrodes. (a) Ag NWs bottom electrode film height image. (b) Ag NWs-MoS_2 bottom electrode film height image.

between graphene and silicon of heterojunction solar cells based on graphene/MoS_2/n-Si in the same year. When comparing the solar cell that contains the MoS_2 layer, the PCE of 1.35% is higher than the PCE of the solar cells without the MoS_2 layer, with a PCE of 0.07%. The use of three-layer graphene increased the efficiency of PCE to 8.0%.

Rehman et al.[95] used the Al_2O_3 layer on the MoS_2 surface to improve the performance of the solar cells based on MoS_2/silicon. The PCE = 5.6% was obtained; this is higher than the conversion efficiency of the solar cell based on MoS_2/silicon without adding the Al_2O_3 layer, which was PCE = 2.21%. Also Saraswat et al.[96] made a solar cell based on TMDCs/silicon and gave highly efficient results and excellent photovoltaic performance. Meanwhile, Krishnamoorthy and Prakasam[97] reported on the simple hydrothermal synthesis of diverse compositions of MoS_2/graphene nanocomposites and their subsequent application in DSSCs. The PCE = 8.92% was for MoS_2/graphene and was higher than the conversion efficiency of MoS_2 without graphene (PCE = 3.36%) because graphene increased the charge collection faster and sensitized the dye better.

Maa et al.[98] described a unique approach to synthesizing layers of MoS_2 on diverse substrates such as n-Si that act as photon absorbing layers. This significantly improved the photovoltaic conversion efficiency of graphene-based Schottky junction solar cells. In heterojunction solar cells based on 2D materials, a comparatively high conversion efficiency of 12% was successfully obtained.

Flexible solar cells were manufactured from MoS_2, which works as a hole transfer layer with a transparent conductive electrode.[99] The PCE of these solar cells depends on the number of MoS_2 layers as well as on the concentration of doping, with the value of the PCE being the highest when the number of layers is ($L_n = 2$) and the concentration of doping is ($n_D = 20$ mM). When the active layer with quantum dots was added to the solar cell installation, the efficiency of the conversion power was increased to 4.23%, and this efficiency was maintained after conducting 1000 cycles of tests, which indicates the mechanical stability of this solar cell.

7 Conclusion

We addressed current advances in the basic studies as well as multiapplications of MOS_2 with a focus on one MOS_2 or multilayer MOS_2 as well as on heterostructures. The nanocomposites showed distinctive and unique properties that cannot be obtained in one material. Recently, there have been a large number of studies and applications of technological uses of thin layered MOS_2.

The MOS_2 thin layer is important in various low-cost optoelectronics applications, such as solar cells, light-emitting diodes, photodetectors, and sensors, due to its excellent optical and electronic properties as well as having an adjustable bandgap. In this review, many studies using MOS_2, graphene, and polymers that were used in many heterogeneous applications using a single layer or more were discussed. The results showed a significant improvement in many applications as photodetectors and solar cells and showed new features, which led to an increase in the efficiency of these electronic devices. Several critical challenges must yet be solved if development is to be maintained at this rate. First, new techniques for doping MOS_2 and similar materials to achieve bipolar and p-type behavior must be devised. Second, knowledge and understanding of how building materials interact optimally with device applications must be investigated. The final challenge is a better understanding of heterojunction structures, especially at the atomic level. To address these challenges, advanced scientific research must be conducted in various disciplines. It is expected that the research and development of MOS_2, graphene, and polymers will be effective and have distinctive and promising results that contribute to the development of many electronic applications in the near future.

References

1. D. Chrisey and G. Hubler, *Pulsed Laser Deposition of Thin Films*, John Wiley & Sons, New York (1994).
2. D. Bauerle, Ed., *Laser Processing and Chemistry*, Springer-Verlag (2000).
3. E. Fogarassy and S. Lazare, *Laser Ablation of Electronic Materials*, North Holland Publishing Company (1992).
4. L. Gallais and J.-Y. Natoli, "Optimized metrology for laser-damage measurement: application to multiparameter study,"*Appl. Opt.* **42**(6), 960–971 (2003).
5. K. Mittal, *Particles on Surfaces*, Vol. 1, Plenum Press, New York (1988).
6. X. Wu et al., **70**, 167–178 (1999).
7. J. Perriere, E. Millon, and E. Fogarassy, *Recent Advances in Laser Processing of Materials*, Elsevier Science (2006).
8. A. Rai et al., "Progress in contact, doping and mobility engineering of MoS_2: an atomically thin 2D semiconductor," *Crystals* **8**(8), 316 (2018).
9. Q. Cui et al., "Material and device architecture engineering toward high performance two-dimensional (2D) photodetectors," *Crystals* **7**(5), 149 (2017).
10. K. M. Freedy and S. J. McDonnell, "Contacts for molybdenum disulfide: interface chemistry and thermal stability," *Materials (Basel)* **13**(3), 693 (2020).
11. K. Roy et al., "Graphene–MoS_2 hybrid structures for multifunctional photoresponsive memory devices," *Nat. Nanotechnol.* **8**(11), 826–830 (2013).
12. M. Rahman et al., "Design and numerical analysis of highly sensitive Au–MoS_2–graphene-based hybrid surface plasmon resonance biosensor," *Opt. Commun.* **396**, 36–43 (2017).
13. H. R. Nalwa, "A review of molybdenum disulfide (MoS_2) based photodetectors: from ultra-broadband, self-powered to flexible devices," *RSC Adv.* **10**(51), 30529–30602 (2020).
14. T. Ahmed et al., "Interplay of charge transfer and disorder in optoelectronic response in graphene/hBN/MoS_2 van der Waals heterostructures," *2D Mater.* **7**(2), 025043 (2020).
15. H. Rashid et al., "Prospects of molybdenum disulfide (MoS_2) as an alternative absorber layer material in thin film solar cells from numerical modeling," *Chalcogenide Lett.* **11**(8), 397–403 (2014).
16. Q. A. Vu et al., "Tuning carrier tunneling in van der Waals heterostructures for ultrahigh detectivity," *Nano Lett.* **17**(1), 453–459 (2017).
17. S. Rathi et al., "Tunable electrical and optical characteristics in monolayer graphene and few-layer MoS_2 heterostructure devices," *Nano Lett.* **15**(8), 5017–5024 (2015).
18. H. Li et al., "Restoring the photovoltaic effect in graphene-based van der Waals heterojunctions towards self-powered high-detectivity photodetectors," *Nano Energy* **57**, 214–221 (2019).
19. D. De Fazio et al., "High responsivity, large-area graphene/MoS_2 flexible photodetectors," *ACS Nano* **10**(9), 8252–8262 (2016).

20. B. Radisavljevic et al., "Single-layer MoS_2 transistors," *Nat. Nanotechnol.* **6**(3), 147–150 (2011).
21. W. M. Haynes, *CRC Handbook of Chemistry and Physics, (Internet Version 2011)*, Taylor Francis Group, Boca Raton, Florida (2011).
22. W. S. Yun et al., "Thickness and strain effects on electronic structures of transition metal dichalcogenides: 2H-MX_2 semiconductors (M = Mo, W; X = S, Se, Te)," *Phys. Rev. B* **85**(3), 033305 (2012).
23. A. T. Dideikin and A. Y. Vul, "Graphene oxide and derivatives: the place in graphene family," *Front. Phys.* **6**, 149 (2019).
24. G. Nagaraju et al., "Hydrothermal synthesis of amorphous MoS_2 nanofiber bundles via acidification of ammonium heptamolybdate tetrahydrate," *Nanosc. Res. Lett.* **2**(9), 461–468 (2007).
25. Y. Li et al., "MoS_2 nanoparticles grown on graphene: an advanced catalyst for the hydrogen evolution reaction," *J. Am. Chem. Soc.* **133**(19), 7296–7299 (2011).
26. B. C. Helmly et al., "Preparation and spectroscopic characterization of MoS_2 and $MoSe_2$ nanoparticles," *Spectrosc. Lett.* **40**(3), 483–492 (2007).
27. B. Li et al., "Preparation of monolayer MoS_2 quantum dots using temporally shaped femtosecond laser ablation of bulk MoS_2 targets in water," *Sci. Rep.* **7**(1), 1–12 (2017).
28. S. Moniri and M. R. Hantehzadeh, "Colloidal synthesis of MoS_2 NPs by nanosecond laser ablation of a bulk MoS_2 target in ethylene glycol solution," *Opt. Quantum Electron.* **53**(5), 1–17 (2021).
29. A. K. Geim and K. S. Novoselov, "The rise of graphene," *Nat. Mater.* **6**, 183–191 (2007).
30. M. Nurunnabi and J. McCarthy, Eds., *Biomedical Applications of Graphene and 2D Nanomaterials*, Elsevier (2019).
31. M. K. Mohammed, A. Al-Nafiey, and G. Al-Dahash, "Manufacturing graphene and graphene-based nanocomposite for piezoelectric pressure sensor application: a review," *Nano Biomed. Eng.* **13**(1), 27–35 (2021).
32. A. Zavabeti et al., "Two-dimensional materials in large-areas: synthesis, properties and applications," *Nano-Micro Lett.* **12**(1), 1–34 (2020).
33. H. Tao et al., "Scalable exfoliation and dispersion of two-dimensional materials—an update," *Phys. Chem. Chem. Phys.* **19**(2), 921–960 (2017).
34. W. Li et al., "Gas sensors based on mechanically exfoliated MoS_2 nanosheets for room-temperature NO_2 detection," *Sensors* **19**(9), 2123 (2019).
35. K. R. Paton et al., "Scalable production of large quantities of defect-free few-layer graphene by shear exfoliation in liquids," *Nat. Mater.* **13**(6), 624–630 (2014).
36. Y. Hernandez et al., "High-yield production of graphene by liquid-phase exfoliation of graphite," *Nat. Nanotechnol.* **3**(9), 563–568 (2008).
37. P. G. Karagiannidis, "Microfluidization of graphite and formulation of graphene-based conductive inks," *ACS Nano* **11**, 2742–2755 (2017).
38. Z. Shen et al., "Preparation of graphene by jet cavitation," *Nanotechnology* **22**, 365306 (2011).
39. J. Yu et al., "Synthesis of two-dimensional materials via chemical vapor deposition," *Chem. Sci.* **6**, 6705–6716 (2015).
40. J. Chen et al., "Chemical vapor deposition of large-size monolayer $MoSe_2$ crystals on molten glass," *J. Am. Chem. Soc.* **139**, 1073–1076 (2017).
41. Z. Yan and B. C. Douglas, "Pulsed laser ablation in liquid for micro-/nanostructure generation," *J. Photochem. Photobiol., C* **13**(3), 204–223 (2012).
42. S. Iijima et al., "Nano-aggregates of single-walled graphitic carbon nano-horns," *Chem. Phys. Lett.*, **309**, 165 (1999).
43. E. Werwa et al., "Synthesis and processing of silicon nanocrystallites using a pulsed laser ablation supersonic expansion method," *Appl. Phys. Lett.* **64**(14), 1821–1823 (1994).
44. P. V. Kazakevich et al., "Laser induced synthesis of nanoparticles in liquids," *Appl. Surf. Sci.* **252**(13), 4373–4380 (2006).
45. V. S. Naik, V. S. P. Bhanudas, and N. N. Ghosh, "A simple aqueous solution based chemical methodology for synthesis of Ag nanoparticles dispersed on mesoporous silicate matrix," *Powder Technol.* **199**(2), 197–201 (2010).

46. Y. Qin et al., "Review of deep ultraviolet photodetector based on gallium oxide," *Chin. Phys. B* **28**, 018501 (2019).
47. W. Tian et al., "Self-powered nanoscale photodetectors," *Small* **13**, 1701848 (2017).
48. H. Qiao et al., "Self-powered photodetectors based on 2D materials," *Adv. Opt. Mater.* **8**, 1900765 (2019).
49. A. De Sanctis et al., "Graphene-based light sensing: fabrication, characterisation, physical properties and performance," *Materials (Basel)* **11**, 1762 (2018).
50. B. Sun et al., "Progress on crystal growth of two-dimensional semiconductors for optoelectronic applications," *Crystals* **8**, 252 (2018).
51. B. Liu et al., "High performance photodetector based on graphene/MoS_2/graphene lateral heterostrurcture with Schottky junctions," *J. Alloys Compd.* **779**, 140–146 (2019).
52. L. Xu et al., "Two-dimensional MoS_2–graphene-based multilayer van Der Waals heterostructures: enhanced charge transfer and optical absorption, and electric-field tunable Dirac point and band gap," *Chem. Mater.* **29**, 5504–5512 (2017).
53. G. Konstantatos, "Current status and technological prospect of photodetectors based on two-dimensional materials," *Nat. Commun.* **9**, 9–11 (2018).
54. Z. Huang et al., "Interfacial gated graphene photodetector with broadband response," *ACS Appl. Mater. Interfaces* **13**, 22796−22805 (2021).
55. Y. S. Shih et al., "Low power photodetectors based on PVA modified reduced graphene oxide hybrid solutions," *Macromol. Rapid Commun.* **43**, 2100854 (2022).
56. Z. Yin et al., "Single-layer MoS_2 phototransistors," *ACS Nano* **6**, 74–80 (2012).
57. O. Lopez-Sanchez et al., "Ultrasensitive photodetectors based on monolayer MoS_2," *Nat. Nanotechnol.* **8**, 497–501 (2013).
58. M. F. Khan et al., "Photocurrent response of MoS_2 field-effect transistor by deep ultraviolet light in atmospheric and N_2 gas environments," *ACS Appl. Mater. Interfaces* **6**, 21645–21651 (2014).
59. D. S. Tsai et al., "Few-layer MoS_2 with high broadband photogain and fast optical switching for use in harsh environments," *ACS Nano* **7**, 3905–3911 (2013).
60. J. Lu et al., "Improved photoelectrical properties of MoS_2 films after laser micromachining," *ACS Nano* **8**, 6334–6343 (2014).
61. V. Selamneni, S. K. Ganeshan, and P. Sahatiya, "All MoS_2 based 2D/0D localized unipolar heterojunctions as flexible broadband (UV-vis-NIR) photodetectors," *J. Mater. Chem. C* **8**(33), 11593–11602 (2020).
62. P. Han et al., "Highly sensitive MoS_2 photodetectors with graphene contacts," *Nanotechnology* **29**, 20LT01 (2018).
63. S. Kumar et al., "High performance UV photodetector based on MoS_2 layers grown by pulsed laser deposition technique," *J. Alloys Compd.* **835**, 155222 (2020).
64. X. Liu et al., "Suspended MoS_2 photodetector using patterned sapphire substrate," *Nano-Microsmall* **17**, 2100246 (2021).
65. Z. Li et al., "Telecom-band waveguide-integrated MoS_2 photodetector assisted by hot electrons," *ACS Photonics* **9**(1), 282–289 (2022).
66. W. Zhang et al., "Synthesis and sensor applications of MoS_2-based nanocomposites," *Nanoscale* **7**(44), 18364–18378 (2015).
67. Z. Huang et al., "Photoelectrochemical-type sunlight photodetector based on MoS_2/graphene heterostructure," *2D Mater.* **2**(3), 035011 (2015).
68. B. Sun et al., "Large-area flexible photodetector based on atomically thin MoS_2/graphene film," *Mater. Des.* **154**, 1–7 (2018).
69. A. Yadav et al., "Poly-(3-hexylthiophene)/graphene composite based organic photodetectors: the influence of graphene insertion," *Thin Solid Films* **675**, 128–135 (2019).
70. N. Chaudhary, M. Khanuja, and S. S. Islam, "Broadband photodetector based on 3D architect of MoS_2–PANI hybrid structure for high photoresponsive properties," *Polymer* **165**, 168–173 (2019).
71. I. Lee et al., "Photoinduced tuning of Schottky barrier height in graphene/MoS_2 heterojunction for ultrahigh performance short channel phototransistor," *ACS Nano* **14**, 7574–7580 (2020).

72. E. Soleimani et al., "Tuning the polymer–graphene interfaces by picric acid molecules to improve the sensitivity of a prepared conductive polymer composite gas detector," *Iran. Polym. J.* **29**(4), 341–350 (2020).
73. M. K. Mohammed et al., "Employment of polymer/graphene-Ag nanocomposite films prepared by PLAL for optoelectric applications," University of Babylon (2021).
74. E. Singh et al., "Atomically thin-layered molybdenum disulfide (MoS_2) for bulk-heterojunction solar cells," *ACS Appl. Mater. Interfaces* **9**(4), 3223–3245 (2017).
75. W. Tang, S. S. Rassay, and N. M. Ravindra, "Electronic and optical properties of transition-metal dichalcogenides," *Madr. J. Nanotechnol. Nanosci.* **2**, 58–64 (2017).
76. M. Bernardi, M. Palummo, and J. C. Grossman, "Extraordinary sunlight absorption and one nanometer thick photovoltaics using two-dimensional monolayer materials," *Nano Lett.* **13**, 3664–3670 (2013).
77. Y. Y. Dou et al., "Nickel phosphide-embedded graphene as counter electrode for dye-sensitized solar cells," *Phys. Chem. Chem. Phys.* **14**, 1339–1342 (2012).
78. H. Jeong et al., "Rapid sintering of MoS_2 counter electrode using near-infrared pulsed laser for use in highly efficient dye-sensitized solar cells," *J. Power Sour.* **330**, 104–110 (2016).
79. A. Antonelou et al., "Facile, Substrate-scale growth of mono- and few-layer homogeneous MoS_2 films on Mo foils with enhanced catalytic activity as counter electrodes in DSSCs," *Nanotechnology* **27**, 045404 (2015).
80. C. K. Cheng and C. K. Hsieh, "Electrochemical deposition of molybdenum sulfide thin films on conductive plastic substrates as platinum-free flexible counter electrodes for dye-sensitized solar cells," *Thin Solid Films* **584**, 52–60 (2015).
81. B. Lei, G. R. Li, and X. P. Gao, "Morphology dependence of molybdenum disulfide transparent counter electrode in dye-sensitized solar cells," *J. Mater. Chem. A* **2**, 3919–3925 (2014).
82. J.-Y. Lin et al., "Hydrothermal synthesis of graphene flakeembedded nanosheet-like molybdenum sulfide hybrids as counter electrode catalysts for dye-sensitized solar cells," *Mater. Chem. Phys.* **143**, 53–59 (2013).
83. C.-J. Liu et al., "Facile synthesis of MoS_2/graphene nanocomposite with high catalytic activity toward triiodide reduction in dye-sensitized solar cells," *J. Mater. Chem.* **22**, 21057–21064 (2012).
84. X. Gu et al., "A solution-processed hole extraction layer made from ultrathin MoS_2 nanosheets for efficient organic solar cells," *Adv. Energy Mater.* **3**, 1262–1268 (2013).
85. X. Li et al., "Solution-processed MoSx as an efficient anode buffer layer in organic solar cells," *ACS Appl. Mater. Interfaces* **5**, 8823–8827 (2013).
86. M. S. Ramasamy et al., "Solution-processed PEDOT: PSS/MoS_2 nanocomposites as efficient hole-transporting layers for organic solar cells," *Nanomaterials (Basel)* **9**, 1328 (2019).
87. X. Yang et al., "Engineering crystalline structures of two-dimensional MoS_2 sheets for high-performance organic solar cells," *J. Mater. Chem. A* **2**, 7727–7733 (2014).
88. J.-M. Yun et al., "Efficient work-function engineering of solution-processed MoS_2 thin-films for novel hole and electron transport layers leading to high-performance polymer solar cells," *J. Mater. Chem. C* **1**, 3777–3783 (2013).
89. X. Hu et al., "Versatile MoS_2 nanosheets in ITO-free and semi-transparent polymer power-generating glass," *Sci. Rep.* **5**, 1–13 (2015).
90. P. Qin et al., "In situ growth of double-layer MoO_3/MoS_2 film from MoS_2 for hole-transport layers in organic solar cell," *J. Mater. Chem. A* **2**, 2742–2756 (2014).
91. X. Yang et al., "Au nanoparticles on ultrathin MoS_2 sheets for plasmonic organic solar cells," *J. Mater. Chem. A* **2**, 14798–14806 (2014).
92. M. K. Chuang, S. S. Yang, and F. C. Chen, "Metal nanoparticle-decorated two-dimensional molybdenum sulfide for plasmonic-enhanced polymer photovoltaic devices," *Materials (Basel)* **8**, 5414–5425 (2015).
93. K. Jiao et al., "The role of MoS_2 as an interfacial layer in graphene/silicon solar cells," *Phys. Chem. Chem. Phys.* **17**, 8182–8186 (2015).
94. Y. Tsuboi et al., "Enhanced photovoltaic performances of graphene/Si solar cells by insertion of a MoS_2 thin film," *Nanoscale* **7**, 14476–14482 (2015).

95. A. U. Rehman et al., "N-MoS_2/p-Si solar cells with Al_2O_3 passivation for enhanced photogeneration," *ACS Appl. Mater. Interfaces* **8**, 29383–29390 (2016).
96. K. C. Saraswat et al., *Low Cost Silicon (Si)/Transition Metal Dichalcogenides (TMDs) Tandem Solar Cells with Goal of >30% Efficiency*, Vol. S18-187, pp. 1–2, Stanford University. Stanford, California (2019).
97. D. Krishnamoorthy and A. Prakasam, "Preparation of MoS_2/graphene nanocomposite-based photoanode for dye-sensitized solar cells (DSSCs)," *Inorg. Chem. Commun.* **118**, 108016 (2020).
98. J. Ma, Y. Yuan, and P. Sun, "Performances enhancement of graphene/n-Si Schottky junction solar cells with dual-functional MoS_2 interfacial layers," *J. Alloys Compd.* **883**, 160898 (2021).
99. D. H. Shin et al., "Enhancement of efficiency and stability in organic solar cells by employing MoS_2 transport layer, graphene electrode, and graphene quantum dots-added active layer," *Appl. Surf. Sci.* **538**, 148155 (2021).

Nagham M. Obaid received her BSc degree in physics from the College of Education at the University of Babylon in 2006 and her MSc degree in laser physics from the College of Science for Women at the University of Babylon in 2016. Now she is a PhD student in the research stage at the College of Science for Women of the University of Babylon. Her scientific interests are in the fields of lasers and their wide applications and she has conducted several research projects in this field.

Amer Al-Nafiey received his BSc degree in physics from the University of Babylon in 1998, his MSc degree in physics from the same university in 2006, and his PhD in nanotechnology from Lille1 University of Science and Technology in 2016. Now, he is an academic researcher and an assistant professor at the College of Science for Women of the University of Babylon. His scientific interests are in the fields focused on nanomaterials, nanomaterials synthesis, material characterization, thin film synthesis, nanostructured materials, nanocomposites, carbon nanomaterials, catalysis, and bio-nanoapplications. He has more than 25 research papers published in international peer-reviewed journals.

Ghalib Al-Dahash received his BSc degree in physics from Al-Mustansiriya University in 1986, his MSc degree in nuclear material physics from the same university in 1992, and his PhD in solid-state physics with a focus on superconductivity from the University of Baghdad in 1998. Now, he is a professor of physics at the College of Science for Women of the University of Babylon. His scientific interests are in the fields of laser material processing and superconductors. He has more than 86 research papers published in international peer-reviewed journals.